Supporting Information

Cyclometallated phosphonium ylide-based iridium(III) photocatalysts

Oussama Fayafrou,[a] Juliette Zanzi,[a] Carine Duhayon ,[a] Jean-Baptiste Sortais,[a] Olivier Baslé,*[a] and Yves Canac*[a]

[a] LCC–CNRS, Université de Toulouse, CNRS, UPS, Toulouse, France.

Table of contents

I) General remarks

All manipulations were performed under an inert atmosphere of dry nitrogen by using standard vacuum line and Schlenk tube techniques. Glassware was dried at 120°C in an oven for at least three hours. THF, Et_2O, pentane, toluene and CH_2Cl_2 were dried using an Innovative Technology solvent purification system. Acetonitrile was dried using a MBraun SPS column. Chromatographic purification was carried out on silica gel (SiO_2, 63−200 μm). ^{1}H, ^{31}P, and ^{13}C NMR spectra were obtained on Bruker AV300, AV400 or NEO600 spectrometers. NMR chemical shifts δ are in ppm, with positive values to high frequency relative to the tetramethylsilane reference for ^{1}H and ^{13}C, and to H_3PO_4 for ^{31}P. If necessary, additional information on the carbon signal attribution was obtained using $^{13}C\{^1H, ^{31}P\}$, *J*-modulated spin−echo (JMOD) $^{13}C\{^1H\}$, $^1H-^{13}C$ HMQC, and/or HMBC experiments. MS spectra (ESI mode) were performed by the mass spectrometry service of the “Institut de Chimie de Toulouse”. Elemental analyses were performed by the elemental analysis service of the LCC-UPR CNRS 8241 with a Perkin Elmer 2400 series II analyzer. Absorption spectra were recorded on PerkinElmer U.V. Spectrometer Lambda 950. Luminescence spectra were obtained with Horiba Jobin Yvon FluoroMax-4 Spectrophotometer. Quantum yield measurements were measured on Hamamatsu spectrometer PL-QY QUANTAURUS QY+. Luminescence lifetimes were recorded on Horiba Fluorolog 3-2iHR320. $[Ir(ppy)_2\text{-}\mu\text{-}Cl]_2$ and $[Ir(dF(CF_3)ppy)_2\text{-}\mu\text{-}Cl]_2$ complexes were synthetized according literature procedure.[1] Phosphonium [**1**](I) was prepared according to a recently reported procedure.[2] All reagent-grade chemicals purchased from commercial sources were used as received.

II) Synthetic procedures

Iridium complex [2a](PF_6):

To a solution of [**1**](I) (100 mg, 0.25 mmol) in THF (10 mL), KHMDS was added dropwise (0.5 M in toluene, 0.6 mL, 0.3 mmol) at –78°C under inert atmosphere. The solution was stirred 20 min at –78°C and then 40 min at –25°C. A solution of $[Ir(ppy)_2\text{-}\mu\text{-}Cl]_2$ (134 mg, 0.13 mmol) in THF (10 mL) was added at –78°C and the mixture was stirred for 16 hours at RT. After evaporation of THF, the mixture was dissolved in CH_2Cl_2/H_2O (1/1) and KPF_6 (138 mg, 0.75 mmol) was added to the biphasic solution. The solution was stirred at RT for 2 hours. The organic phase was then separated and dried on Na_2SO_4. A separation by chromatography column on silica gel was carried out using (95-90% DCM/10-5% Acetone) as eluent. The desired complex [**2a**](PF_6) was obtained as a yellow powder (186 mg, 82%). Recrystallization from CH_2Cl_2/Et_2O at RT gave yellow crystals suitable for X-ray diffraction analysis. ^{31}P NMR (162 MHz, CD_2Cl_2, 25°C): δ 50.2 (s), –144.5 (hept, J_{PF} = 712.8 Hz). ^{1}H NMR (400 MHz,

CD_2Cl_2, 25°C): δ 8.58 (d, J_{HH} = 5.9 Hz, 1H, CH_{Ar}), 8.16 (d, J_{HH} = 5.4 Hz, 1H, CH_{Ar}), 8.04 (td, J_{HH} = 7.9 Hz, J_{HP} = 3.5 Hz, 1H, CH_{Ar}), 7.99 (d, J_{HH} = 8.2 Hz, 1H, CH_{Ar}), 7.90 (d, J_{HH} = 8.2 Hz, 1H, CH_{Ar}), 7.83–7.74 (m, 3H, CH_{Ar}), 7.73–7.55 (m, 6H, CH_{Ar}), 7.51–7.46 (m, 3H, CH_{Ar}), 7.40–7.28 (m, 5H, CH_{Ar}), 7.03 (t, J_{HH} = 7.2 Hz, 1H, CH_{Ar}), 6.98 (t, J_{HH} = 6.0 Hz, 1H, CH_{Ar}), 6.89 (t, J_{HH} = 7.6 Hz, 2H, CH_{Ar}), 6.75 (t, J_{HH} = 7.4 Hz, 1H, CH_{Ar}), 6.52 (t, J_{HH} = 7.4 Hz, 1H, CH_{Ar}), 6.31 (d, J_{HH} = 7.5 Hz, 1H, CH_{Ar}), 6.21 (d, J_{HH} = 7.7 Hz, 1H, CH_{Ar}), 1.67 (dd, J_{HH} = 14.4 Hz, J_{HP} = 8.8 Hz, 1H, CH_2), 1.13 (dd, J_{HH} = 14.4 Hz, J_{HP} = 10.8 Hz, 1H, CH_2). ^{13}C NMR (101 MHz, CD_2Cl_2, 25°C): δ 170.4 (s, C_{Ar}), 167.7 (s, C_{Ar}), 164.0 (d, J = 2.0 Hz, C_{Ar}), 159.2 (d, J_{CP} = 124.1 Hz, C_{Ar}), 154.7 (d, J_{CP} = 10.3 Hz, CH_{Ar}), 149.9 (s, CH_{Ar}), 148.5 (s, CH_{Ar}), 148.1 (d, J_{CP} = 4.7 Hz, C_{Ar}), 144.4 (s, C_{Ar}), 143.0 (s, C_{Ar}), 138.0 (s, CH_{Ar}), 137.9 (d, J_{CP} = 8.4 Hz, CH_{Ar}), 137.0 (s, CH_{Ar}), 134.7 (d, J_{CP} = 15.5 Hz, CH_{Ar}), 134.6 (s, CH_{Ar}), 134.5 (s, CH_{Ar}), 132.4 (d, J_{CP} = 10.3 Hz, CH_{Ar}), 132.1 (d, J_{CP} = 9.8 Hz, CH_{Ar}), 131.5 (s, CH_{Ar}), 131.2 (s, CH_{Ar}), 130.8 (d, J_{CP} = 12.2 Hz, CH_{Ar}), 130.7 (d, J_{CP} = 12.2 Hz, CH_{Ar}), 130.4 (d, J_{CP} = 2.6 Hz, CH_{Ar}), 130.0 (s, CH_{Ar}), 127.4 (d, J_{CP} = 71.9 Hz, C_{Ar}), 125.3 (s, CH_{Ar}), 124.6 (s, CH_{Ar}), 123.2 (d, J_{CP} = 76.8 Hz, C_{Ar}), 123.0 (s, CH_{Ar}), 122.6 (s, CH_{Ar}), 122.4 (s, CH_{Ar}), 121.2 (s, CH_{Ar}), 120.3 (s, CH_{Ar}), 119.7 (s, CH_{Ar}), –2.6 (d, J_{CP} = 20.8 Hz, CH_2). MS (ES$^+$): *m/z*: 778.2 $[M - PF_6]^+$; HRMS (ES$^+$): *m/z*: calculated for $C_{40}H_{32}N_3PIr^+$: 778.1963, found: 778.1973, εr = 1.3 ppm. Elemental analysis for $C_{40}H_{32}F_6N_3P_2Ir$: calcd, C 52.06, H 3.50, N 4.55; found: C 51.71, H 3.49, N 4.48.

Iridium complex [2b][(PF_6):

To a solution of [**1**](I) (100 mg, 0.25 mmol) in THF (10 mL), KHMDS was added dropwise (0.5 M in toluene, 0.6 mL, 0.3 mmol) at –78°C under inert atmosphere. The solution was stirred 20 min at –78°C and then 40 min at –25°C. A solution of $[Ir(dF(CF_3)ppy)_2\text{-}\mu\text{-}Cl]_2$ (184 mg, 0.13 mmol) in THF (10 mL) was added at –78°C and the mixture was stirred for 16 hours at RT. After evaporation of THF, the mixture was dissolved in CH_2Cl_2/H_2O (1/1) and KPF_6 (138 mg, 0.75 mmol) was added to the biphasic solution. The solution was stirred at RT for 2 hours. The organic phase was then separated and dried on Na_2SO_4. A separation by chromatography column on silica gel was carried out using (97% DCM/3% Acetone) as eluent. The desired complex [**2b**](PF_6) was obtained as a yellow powder (209 mg, 75%). Recrystallization from CH_2Cl_2/Et_2O at RT gave crystals suitable for X-ray diffraction analysis. ^{31}P NMR (162 MHz, CD_2Cl_2, 25°C): δ 51.3 (s), –144.6 (hept, J_{PF} = 709.6 Hz). ^1H NMR (400 MHz, CD_2Cl_2, 25°C): δ 8.97 (s, 1H, CH_{Ar}), 8.58 (br d, J_{HH} = 8.9 Hz, 1H, CH_{Ar}), 8.48 (br d, J_{HH} = 8.9 Hz, 1H, CH_{Ar}), 8.27–8.20 (m, 2H, CH_{Ar}), 8.11 (br d, J_{HH} = 8.8 Hz, 1H, CH_{Ar}), 7.92 (br d, J_{HH} = 8.8 Hz, 1H, CH_{Ar}), 7.86–7.61 (m, 6H, CH_{Ar}), 7.57–7.50 (m, 2H, CH_{Ar}), 7.47 (s, 1H, CH_{Ar}), 7.37 (dd, J_{HH} = 7.6 Hz, J_{HP} = 13.2 Hz, 2H, CH_{Ar}), 7.28 (dd, J_{HH} = 8.0 Hz, J_{HP} = 12.8 Hz, 2H, CH_{Ar}), 6.63 (br t,

J_{HH} = 10.7 Hz, 1H, CH_{Ar}), 6.52 (br t, J_{HH} = 10.9 Hz, 1H, CH_{Ar}), 5.76 (br d, J_{HH} = 8.0 Hz, 1H, CH_{Ar}), 5.64 (br d, J_{HH} = 8.5 Hz, 1H, CH_{Ar}), 1.76 (dd, J_{HH} = 15.2 Hz, J_{HP} = 9.2 Hz, 1H, CH_2), 1.27 (dd, J_{HH} = 15.2 Hz, J_{HP} = 11.6 Hz, 1H, CH_2). ^{13}C NMR (101 MHz, CD_2Cl_2, 25°C): δ 170.6 (d, J_{CF} = 7.6 Hz, C_{Ar}), 169.8 (br s, C_{Ar}), 168.2 (d, J_{CF} = 6.7 Hz, C_{Ar}), 165.9 (dd, J_{CF} = 12.9 and 260.0 Hz, C_{Ar}), 164.6 (dd, J_{CF} = 12.6 and 259.3 Hz, C_{Ar}), 163.6 (dd, J_{CF} = 10.5 and 261.9 Hz, C_{Ar}), 162.7 (dd, J_{CF} = 10.2 and 262.0 Hz, C_{Ar}), 158.6 (d, J_{CP} = 121.3 Hz, C_{Ar}), 154.9 (d, J_{CP} = 10.0 Hz, CH_{Ar}), 153.0 (d, J_{CP} = 4.9 Hz, C_{Ar}), 152.9 (d, J_{CP} = 4.7 Hz, C_{Ar}), 146.6 (q, J_{CF} = 4.5 Hz, CH_{Ar}), 145.1 (q, J_{CF} = 4.8 Hz, CH_{Ar}), 139.6 (d, J_{CP} = 8.4 Hz, CH_{Ar}), 136.6 (d, J_{CF} = 3.3 Hz, CH_{Ar}), 135.7 (d, J_{CP} = 18.2 Hz, CH_{Ar}), 135.5 (s, CH_{Ar}), 135.3 (d, J_{CP} = 2.9 Hz, CH_{Ar}), 135.2 (d, J_{CP} = 3.0 Hz, CH_{Ar}), 132.1 (d, J_{CP} = 10.9 Hz, CH_{Ar}), 131.8 (d, J_{CP} = 9.8 Hz, CH_{Ar}), 131.6 (d, J_{CP} = 2.6 Hz, CH_{Ar}), 131.1 (d, J_{CP} = 12.1 Hz, CH_{Ar}), 131.0 (d, J_{CP} = 12.1 Hz, CH_{Ar}), 126.9 (q, J_{CF} = 2.6 Hz, C_{Ar}), 126.0 (d, J_{CP} = 73.8 Hz, C_{Ar}), 125.7 (q, J_{CF} = 34.2 Hz, C_{Ar}), 125.1 (q, J_{CF} = 34.7 Hz, C_{Ar}), 124.3 (d, J_{CF} = 22.3 Hz, CH_{Ar}), 123.9 (d, J_{CF} = 20.9 Hz, CH_{Ar}), 121.4 (d, J_{CP} = 78.4 Hz, C_{Ar}), 122.5 (q, J_{CF} = 271.4 Hz, CF_3), 122.1 (q, J_{CF} = 270.4 Hz, CF_3), 113.8 (dd, J_{CF} = 3.1 and 11.2 Hz, CH_{Ar}), 113.7 (dd, J_{CF} = 2.9 and 10.0 Hz, CH_{Ar}), 99.7 (t, J_{CF} = 27.1 Hz, CH_{Ar}), 98.3 (t, J_{CF} = 26.9 Hz, CH_{Ar}), –1.6 (d, J_{CP} = 23.2 Hz, CH_2). MS (ES^+): *m/z*: 986.1 $[M - PF_6]^+$; HRMS (ES^+): *m/z*: calculated for $C_{42}H_{26}N_3F_{10}PIr^+$: 986.1334, found: 986.1347, εr = 1.3 ppm. Elemental analysis for $C_{42}H_{26}F_{16}N_3P_2Ir$: calcd, C 44.61, H 2.32, N 3.72; found: C 44.11, H 2.12, N 3.59.

III) X-Ray Diffraction

Single crystals suitable for X-ray diffraction were coated with paratone oil and mounted onto the goniometer. The X-ray crystallographic data were obtained at low temperature from a Rigaku Synergy diffractometer (CuKα), equipped with an Oxford Cryosystem. The structures have been solved by direct methods using SHELXT[3] and refined by means of least-square procedures on F^2 using CRYSTALS.[4] The scattering factors for all the atoms were used as listed in the International Tables for X-ray Crystallography.[5] Absorption correction was performed using a multi-scan procedure. All non-hydrogen atoms were refined anisotropically. The H atoms were usually located in a difference map, but those attached to carbon atoms were systematically repositioned geometrically. The H atoms were initially refined with soft restraints on the bond lengths and angles to regularize their geometry and Uiso (H) (in the range 1.2-1.5 times Ueq of the parent atom), after which the positions were refined with riding constraints. Crystallographic information for all the complexes are gathered in Table S1; the CIF files are also available from The Cambridge Crystallographic Data Centre (www.ccdc.cam.ac.uk/data_request/cif) under the references CCDC-2443033 and 2443034.

	[**2a**](PF_6)	[**2b**](PF_6)
Formula	$\mathrm{C_{44}\,H_{42}\,F_6\,Ir\,N_3\,O\,P_2}$	$\mathrm{C_{42}\,H_{26}\,F_{16}\,Ir\,N_3\,P_2}$
M_w (g mol^{-1})	996.99	1130.82
T(K)	100	100
Crystal system	triclinic	monoclinic
Space group	P-1	P 2_1/n
a (Å)	10.7418(2)	13.2187(2)
b (Å)	13.3809(2)	15.4350(2)
c (Å)	15.7147(2)	20.4572(3)
α (°)	103.6030(10)	90
β (°)	109.915(2)	108.506(2)
γ (°)	91.657(2)	90
V (Å^3)	2049.36(6)	3958.07(11)
Z	2	4
$\rho_{calcd.}$	1.616	1.898
μ (mm^{-1})	7.608	8.331
Collected reflns	54876	64492
Unique reflns	8276	8547
R_{int}	0.045	0.054
Nb of parameters	514	577
Nb of reflns($I \geq 2\sigma$)	0.0322	0.0285
Final R, wR ($I \geq 2\sigma$)	0.0837	0.0724
R, wR (all data)	0.0333/0.0853	0.0303/0.0735
$\Delta\rho_{min}$/ $\Delta\rho_{max}$	-1.66/1.57	-0.78/1.31
GOF	1.010	0.992
CCDC Dep. Number	2443033	2443034

Table S1. Crystallographic table for complexes [**2a**](PF_6) and [**2b**](PF_6).

IV) Photophysical experiments

1) UV-Vis and photoluminescence spectra

Absorption spectra were recorded on PerkinElmer U.V. Spectrometer Lambda 950, in a quartz cuvette (10x10 mm light path) with a screw-cap, in degassed CH_2Cl_2, at 5.10^{-5} M with a scan range of 800 nm to 250 nm at a scan rate of 250 nm/min at room temperature.

Luminescence spectra were obtained with Horiba Jobin Yvon FluoroMax-4 Spectrophotometer, in a quartz cuvette (10x10 mm light path) with a screw-cap, in degassed CH_2Cl_2, at 5.10^{-5} M, at room temperature, with a spectral window from 450 nm to 900 nm, an excitation wavelength at 430 nm, an increment of 1.00 nm and an integration time of 0.10 s.

2) Excited state lifetimes

Luminescence lifetimes were recorded on Horiba Fluorolog 3-2iHR320 equipped with the NanoLED module for TCSPC (Time Correlated Single Photon Counting) lifetime measurements. Samples were excited with a $\lambda = 449$ nm NanoLED. Emission was recorded at 506 nm and 486 nm respectively for [**2a**](PF_6) and [**2b**](PF_6) samples, with a measurement range of 13 microseconds and with a max signal bellow than 2.00%. A 0.01% solution of LUDOX AS-40 colloidal silica (40 wt. % suspensions in H_2O) in purified water was used as reference. Photocatalyst solution were prepared with a concentration around 10^{-5} M in CH_2Cl_2 and placed in a quartz cuvette (10x10 mm light path) with a screw-cap. Samples were degassed for 10 minutes to remove oxygen and avoid the triplet excited-state quenching. The software DAS 6 was used to perform a monoexponential fitting analysis to calculate the lifetimes (Figure S1).

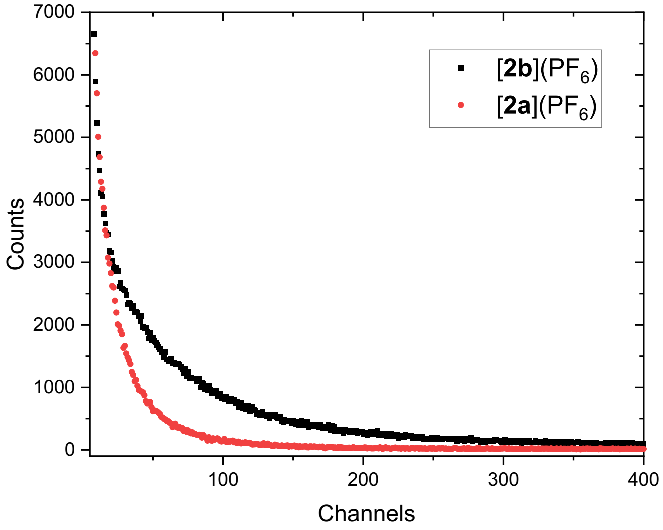

Figure S1. Excited-state life times of Ir(III) complexes [**2a**](PF_6) and [**2b**](PF_6) in CH_2Cl_2.

3) Luminescence quantum yields

Quantum yield measurements were measured on Hamamatsu spectrometer PL-QY QUANTAURUS QY+. Samples were prepared with a concentration of 10^{-5} M in CH_2Cl_2 and placed in 1 ml cylindrical glass cuvette. The solution was degassed directly into the cuvette for 2.5 min just before the analysis.

4) Photostability

The evaluation of the photostability of the two complexes [**2a**](PF_6) and [**2b**](PF_6) was carried out using ^{1}H NMR spectroscopy. A dry NMR tube was prepared by introducing the catalyst, along with 1,3,5-trimethoxybenzene as an internal standard. Homogeneity was achieved by adding dry, degassed CD_2Cl_2. For photostability measurements, the absorbance was adjusted to 21 during the photostability study to ensure identical photon absorption for both photocatalysts. The ^{1}H NMR spectra were initially recorded at t = 0 as a reference.

Subsequently, the samples were exposed to blue LED irradiation in a photoreactor at λ = 460 nm, and their degradation was monitored by analyzing the ^{1}H NMR spectra at different time intervals. For each analysis, four signals were integrated, and the average of these four integrations as a function of time was used to plot the curve (Figures S2-S4).

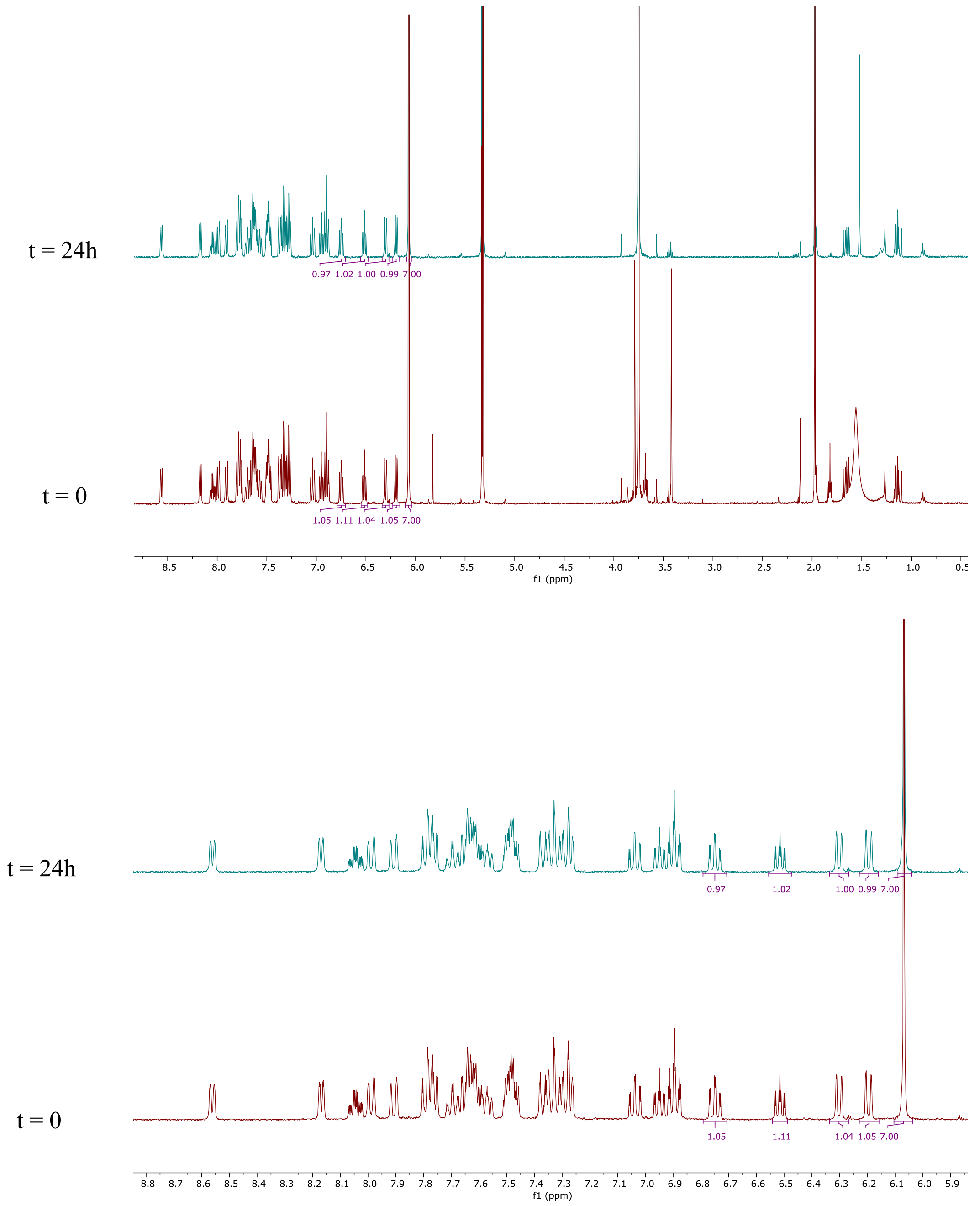

Figure S2: Photostability of Ir(III) complex [**2a**](PF_6) estimated by ^{1}H NMR.

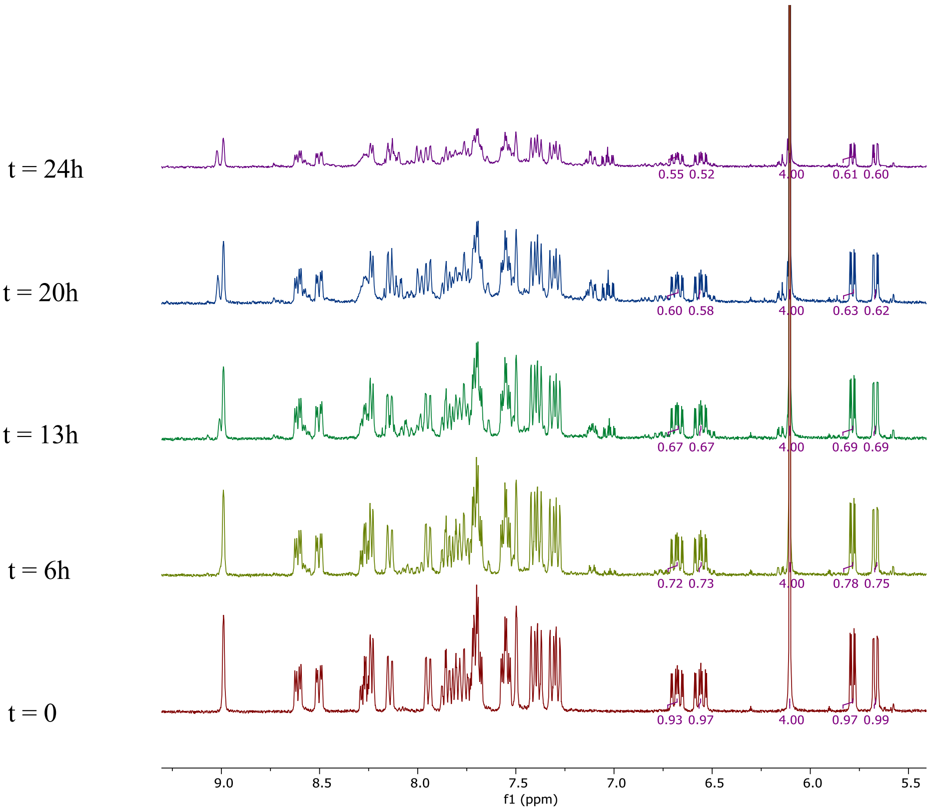

Figure S3: Photostability of Ir(III) complex [**2b**](PF_6) estimated by ^{1}H NMR.

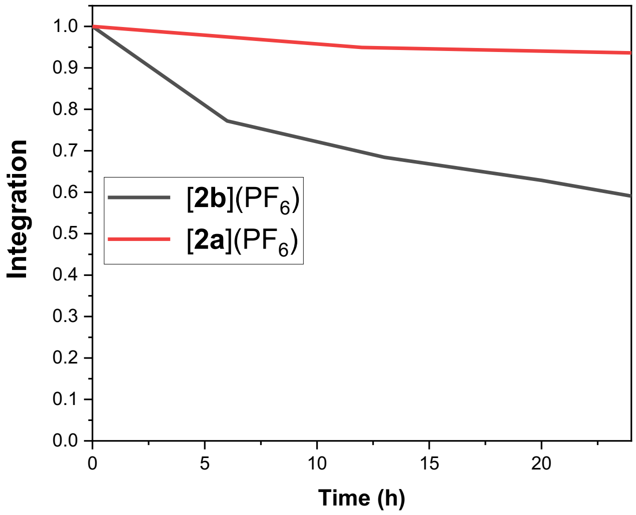

Figure S4: Comparative photostability of Ir(III) complexes [**2a**](PF_6) and [**2b**](PF_6) estimated by ^{1}H NMR.

V) Electrochemical data

Voltammetric measurements were carried out with a potentiostat Autolab PGSTAT100 controlled by GPES 4.09 software. Experiments were performed at RT in a homemade airtight three-electrode cell consisting of a Pt working electrode (d = 0.5 mm), a platinum wire (S = 1 cm^2) as counter electrode, and a saturated calomel electrode (*SCE*) separated from the solution by a bridge compartment as a reference. Before each measurement, the working electrode was cleaned with a polishing machine (Presi P230, P4000). The measurements were carried out in dry CH_2Cl_2 under argon atmosphere using 0.1 M [*n*Bu_4N](PF_6) (Fluka, 99% puriss electrochemical grade) as supporting electrolyte and typically 10^{-3} M sample concentration.

	E_{00} (eV)[a]	$E^{1/2}(Ir^{3+/4+})$ (V)[b]	$E^{1/2}(Ir^{3+/2+})$ (V)[b]	$E(Ir^{3+*/4+})$ (V)	$E(Ir^{3+*/2+})$ (V)
[**2a**](PF_6)	2.45	1.04	–1.59	–1.41	0.86

[a] E_{00} was estimated from the λ_{max} values on emission spectra in CH_2Cl_2.

[b] Redox potentials (V) are given vs saturated calomel electrode (SCE).

Table S2. Ground-state and excited-state redox potentials for complex [**2a**](PF_6) in CH_2Cl_2.

	E_{00} (eV)[a]	$E^{1/2}(Ir^{3+/4+})$ (V)[b]	$E^{1/2}(Ir^{3+/2+})$ (V)[b]	$E(Ir^{3+*/4+})$ (V)	$E(Ir^{3+*/2+})$ (V)
[**2b**](PF_6)	2.55	1.55	–1.43	–1.00	1.12

[a] E_{00} was estimated from the λ_{max} values on emission spectra in CH_2Cl_2.

[b] Redox potentials (V) are given vs saturated calomel electrode (SCE).

Table S3. Ground-state and excited-state redox potentials for complex [**2b**](PF_6) in CH_2Cl_2.

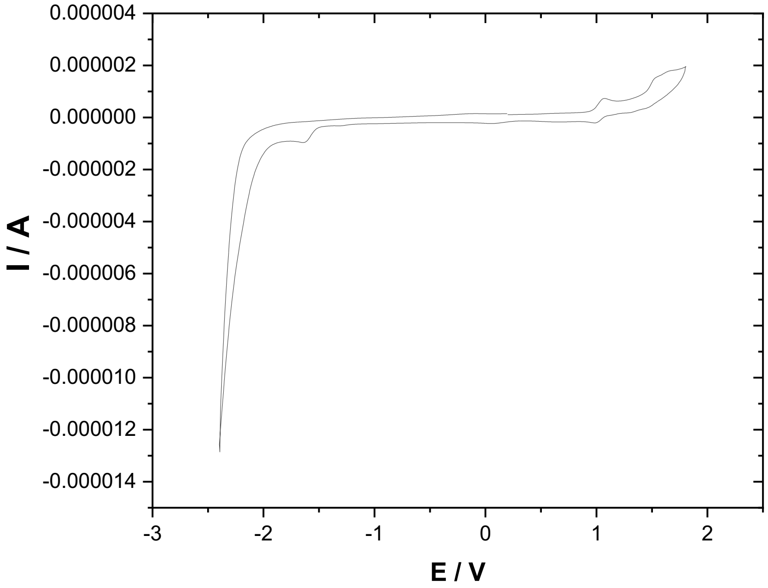

Figure S5. Cyclic voltammogram of Ir(III) complex [**2a**](PF_6) in CH_2Cl_2 (sweep rate = 200 mV/s).

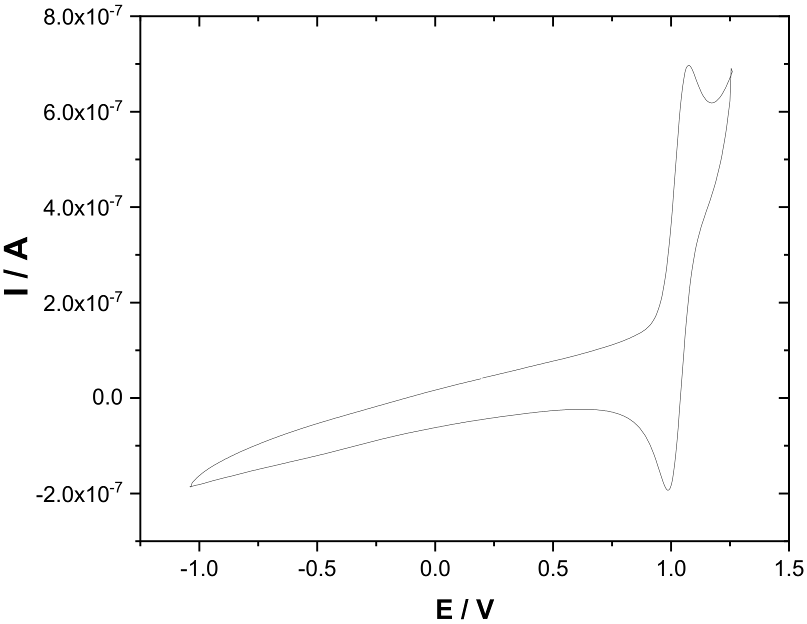

Figure S6. Zoom on oxidation potentials for Ir(III) complex [**2a**](PF_6) in CH_2Cl_2.

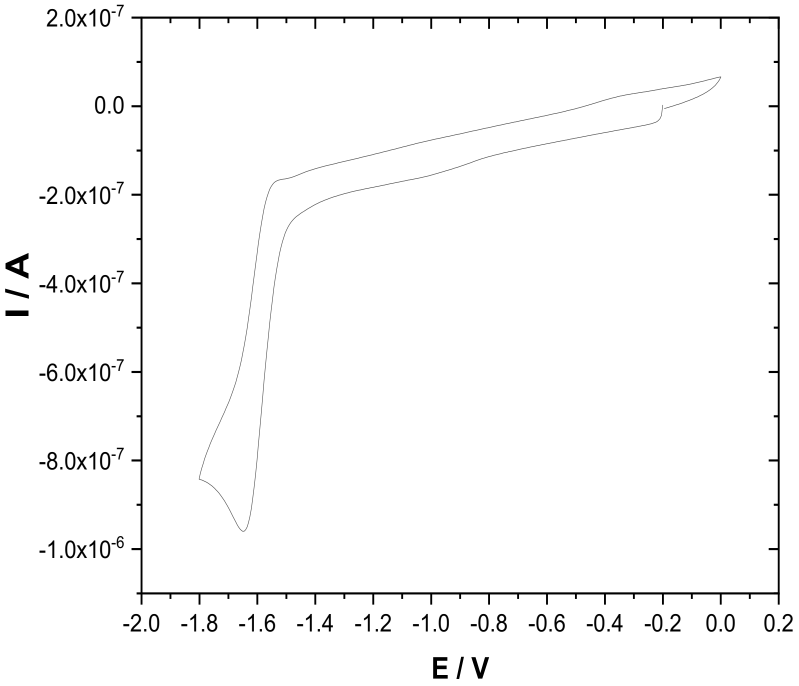

Figure S7. Zoom on reduction potentials for Ir(III) complex [**2a**](PF_6) in CH_2Cl_2.

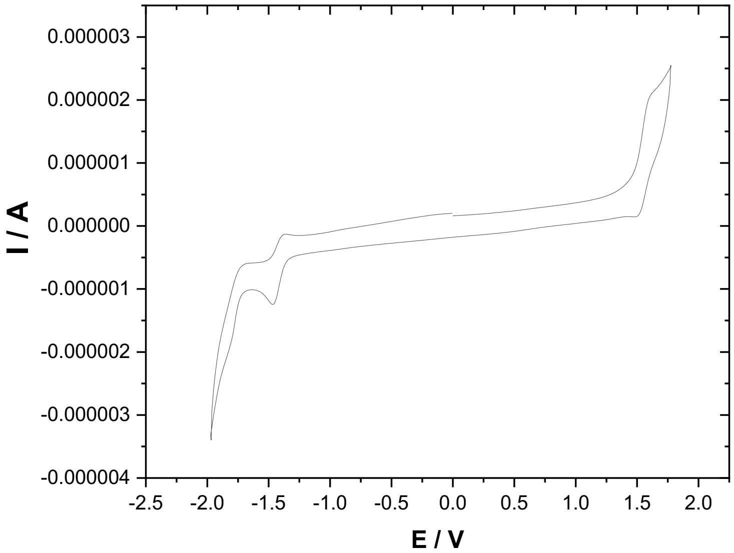

Figure S8. Cyclic voltammogram of Ir(III) complex [**2b**](PF_6) in CH_2Cl_2 (sweep rate = 200 mV/s).

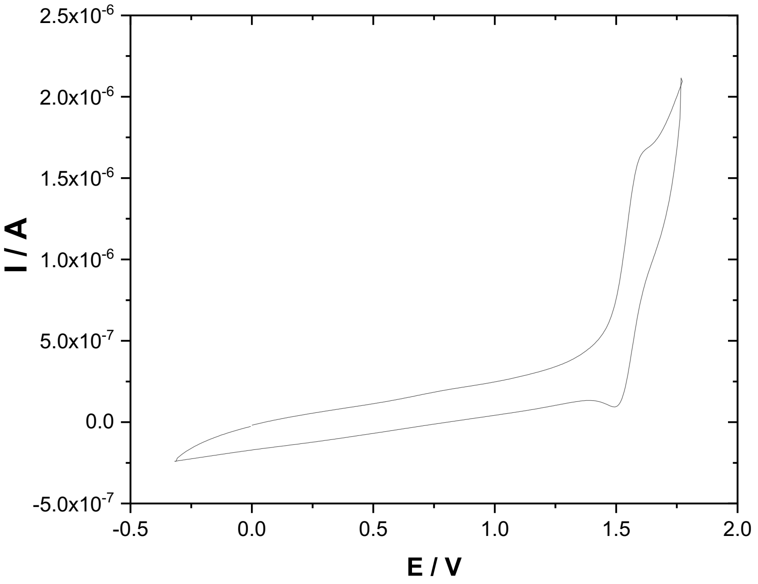

Figure S9. Zoom on oxidation potentials for Ir(III) complex [**2b**](PF_6) in CH_2Cl_2.

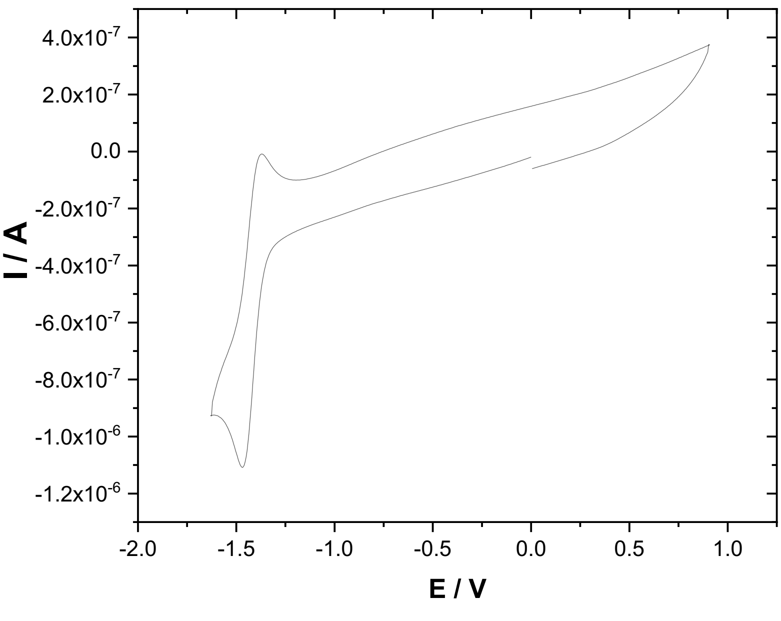

Figure S10. Zoom on reduction potentials for Ir(III) complex [**2b**](PF_6) in CH_2Cl_2.

VI) Catalytic procedures

a) General procedure for [2+2] intermolecular cycloaddition

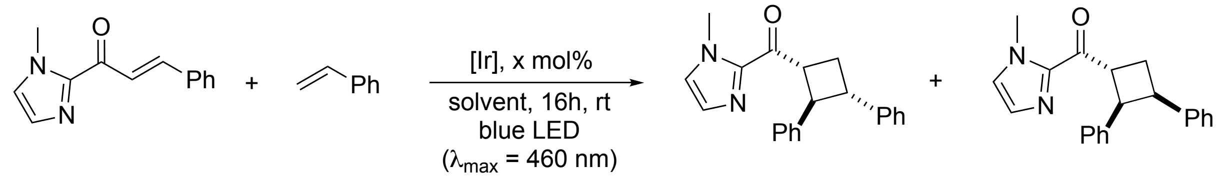

A 2 mL vial was charged with the catalyst (x mol%) and *α,β*-unsaturated substrate (0.1 mmol, 1 equiv.). Dry and degassed solvent was added resulting in a homogeneous mixture. Styrene (1 mmol, 10.0 equiv.) was then added and the vial was purged with argon, sealed and placed under irradiation for 16 h. 1,3,5-trimethoxybenzene was added as internal standard to calculate the yield by ^{1}H NMR.

Table S4. Results of optimization for [2+2] intermolecular cycloaddition.

Solvent	Time (h)	Catalyst	Charge (mol%)	Concentration (M)	Yield (%)
CH_2Cl_2	16	**2a**	0.5	0.5	72 (50/22)
CH_2Cl_2	16	**2a**	0.05	1	35 (26/9)
CH_2Cl_2	16	**2a**	0.05	0.5	28 (26/9)
CH_2Cl_2	16	**2a**	0.01	0.5	15 (10/5)
CH_3CN	16	**2a**	0.5	0.5	58 (39/19)
CH_3CN	16	**2a**	0.05	1	20 (13/7)
CH_3CN	16	**2a**	0.05	0.5	22 (14/8)
CH_3CN	16	**2a**	0.01	0.5	13 (8/5)
CH_2Cl_2	16	**2b**	2	0.1	72 (51/21)
CH_2Cl_2	16	**2b**	1	0.1	72 (51/21)
CH_2Cl_2	16	**2b**	0.5	0.1	65 (46/19)
CH_2Cl_2	16	**2b**	0.5	0.2	77 (54/23)
CH_2Cl_2	16	**2b**	0.5	0.5	70 (49/21)
CH_2Cl_2	16	**2b**	0.1	0.5	74 (53/21)
CH_2Cl_2	16	**2b**	0.05	0.5	70 (50/20)
CH_2Cl_2	16	**2b**	0.01	0.5	67 (50/17)
CH_2Cl_2	16	**2b**	0.5	1	61(43/18)
CH_2Cl_2	16	**2b**	0.1	1	66 (47/19)
CH_2Cl_2	16	**2b**	0.05	1	58 (41/17)
CH_3CN	16	**2b**	1	0.1	79(53/26)
CH_3CN	16	**2b**	0.5	0.1	71(46/25)
CH_3CN	16	**2b**	0.1	0.1	45 (29/16)
CH_3CN	16	**2b**	0.05	0.1	32 (21/11)
CH_3CN	16	**2b**	0.5	0.5	76 (50/26)
CH_3CN	16	**2b**	0.1	0.5	76 (50/26)
CH_3CN	16	**2b**	0.05	0.5	74 (50/24)
CH_3CN	16	**2b**	0.01	0.5	53 (37/16)
CH_3CN	16	**2b**	0.5	1	75 (50/24)
CH_3CN	16	**2b**	0.1	1	75 (54/21)
CH_3CN	16	**2b**	0.05	1	75 (50/25)

Yield in % was determined by ^{1}H NMR using 1,3,5-trimethylbenzene as an internal standard.

b) General procedure for [2+2] intramolecular cycloaddition

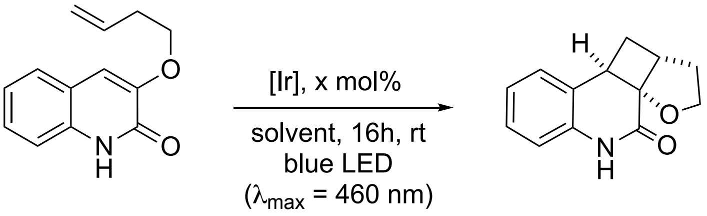

A 2 mL vial was loaded with the catalyst (x mol%) and the quinolone derivative (0.05 mmol, 1 equiv.). Dry, degassed solvent was then added. The vial was purged with argon, sealed, and irradiated for 16 hours. 1,3,5-trimethoxybenzene was subsequently added as an internal standard to determine the yield via ^{1}H NMR spectroscopy.

Table S5. Results of optimization for [2+2] intramolecular cycloaddition.

Solvent	Time (h)	Catalyst	Charge (mol%)	Concentration (M)	Yield (%)
CH_2Cl_2	16	**2a**	0.5	0.5	5
CH_3CN	16	**2a**	0.5	0.5	2
CH_2Cl_2	16	**2b**	2	0.1	92
CH_2Cl_2	16	**2b**	1	0.1	80
CH_2Cl_2	16	**2b**	0.5	0.1	70
CH_2Cl_2	16	**2b**	0.1	0.1	62
CH_2Cl_2	16	**2b**	0.05	0.1	28
CH_2Cl_2	16	**2b**	0.5	0.2	72
CH_2Cl_2	16	**2b**	1	0.5	100
CH_2Cl_2	16	**2b**	0.5	0.5	100
CH_2Cl_2	16	**2b**	0.1	0.5	58
CH_2Cl_2	16	**2b**	0.05	0.5	24
CH_3CN	16	**2b**	1	0.1	96
CH_3CN	16	**2b**	0.5	0.1	86
CH_3CN	16	**2b**	0.1	0.1	19
CH_3CN	16	**2b**	0.05	0.1	6
CH_3CN	16	**2b**	1	0.5	96
CH_3CN	16	**2b**	0.5	0.5	85
CH_3CN	16	**2b**	0.1	0.5	18
CH_3CN	16	**2b**	0.05	0.5	7
CH_2Cl_2	16	**Ir(ppy)$_3$**	0.5	0.5	80
CH_2Cl_2	16	**Ir(ppy)$_3$**	0.1	0.5	43
CH_2Cl_2	16	**Ir(ppy)$_3$**	0.05	0.5	20

Yield in % was determined by ^{1}H NMR using 1,3,5-trimethylbenzene as an internal standard.

c) General procedure for reductive cross-coupling of *N*-benzylideneaniline with methyl acrylate

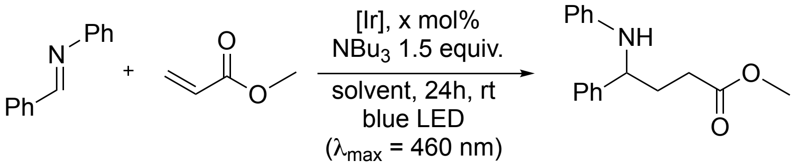

In an oven-dried vial equipped with a magnetic stir bar, the catalyst (x mol%), *N*-benzylideneaniline 1 (0.1 mmol, 1.0 equiv.), and methyl acrylate 2 (0.3 mmol, 3.0 equiv.) were added. The vial was sealed with a septum and subjected to three vacuum/argon cycles to purge it. Degassed solvent (1 mL) and NBu_3 (36 µL, 0.15 mmol, 1.5 equiv.) were then introduced. The vial was placed in a photoreactor with blue LEDs and irradiated for 24 hours. Upon complete conversion, the reaction mixture was concentrated under reduced pressure. 1,3,5-trimethoxybenzene was added as internal standard to calculate the yield by ^{1}H NMR.

Table S6. Results of optimization for reductive cross-coupling.

Solvent	Time (h)	Catalyst	Charge (mol%)	Concentration (M)	Yield (%)
EtOH	24	**2a**	2	0.1	8
DMF	24	**2a**	2	0.1	20
CH_3CN	24	**2a**	2	0.1	53
CH_3CN	24	**2b**	2	0.1	81
DMF	24	**2b**	2	0.1	71
EtOH	24	**2b**	2	0.1	87 (79)
EtOH	24	**2b**	1	0.1	60
EtOH	24	**2b**	1	0.5	47

Yield in % was determined by ^{1}H NMR using 1,3,5-trimethylbenzene as an internal standard. Between brackets, isolated yield after column chromatography on silica gel.

Synthesis and characterization of methyl 4-phenyl-4-(phenylamino)butanoate

Prepared following the general procedure, the crude reaction mixture was purified by column chromatography on silica gel using a pentane/ethyl acetate (9:1) eluent to yield the title compound as a white solid (22 mg, 79%). ^{1}H NMR (400 MHz, $CDCl_3$): δ 7.36–7.30 (m, 4H, H_{Ar}), 7.24–7.20 (m, 1H, H_{Ar}), 7.09 (t, J = 8.0 Hz, 2H, H_{Ar}), 6.64 (t, J = 7.3 Hz, 1H, H_{Ar}), 6.52 (d, J = 7.7 Hz, 2H, H_{Ar}), 4.38 (t, J = 6.8 Hz, 1H, CH), 4.26 (br s, 1H, NH), 3.67 (s, 3H, CH_3), 2.43 (t, J = 7.2 Hz, 2H, CH_2), 2.21–2.06 (m, 2H, CH_2); ^{13}C NMR (101 MHz, $CDCl_3$): δ 174.1, 147.3, 143.2, 129.2, 128.8, 127.4, 126.5, 117.5, 113.4, 57.9, 51.9, 33.3, 31.2 ppm. Spectroscopic data were consistent with the literature data.[6]

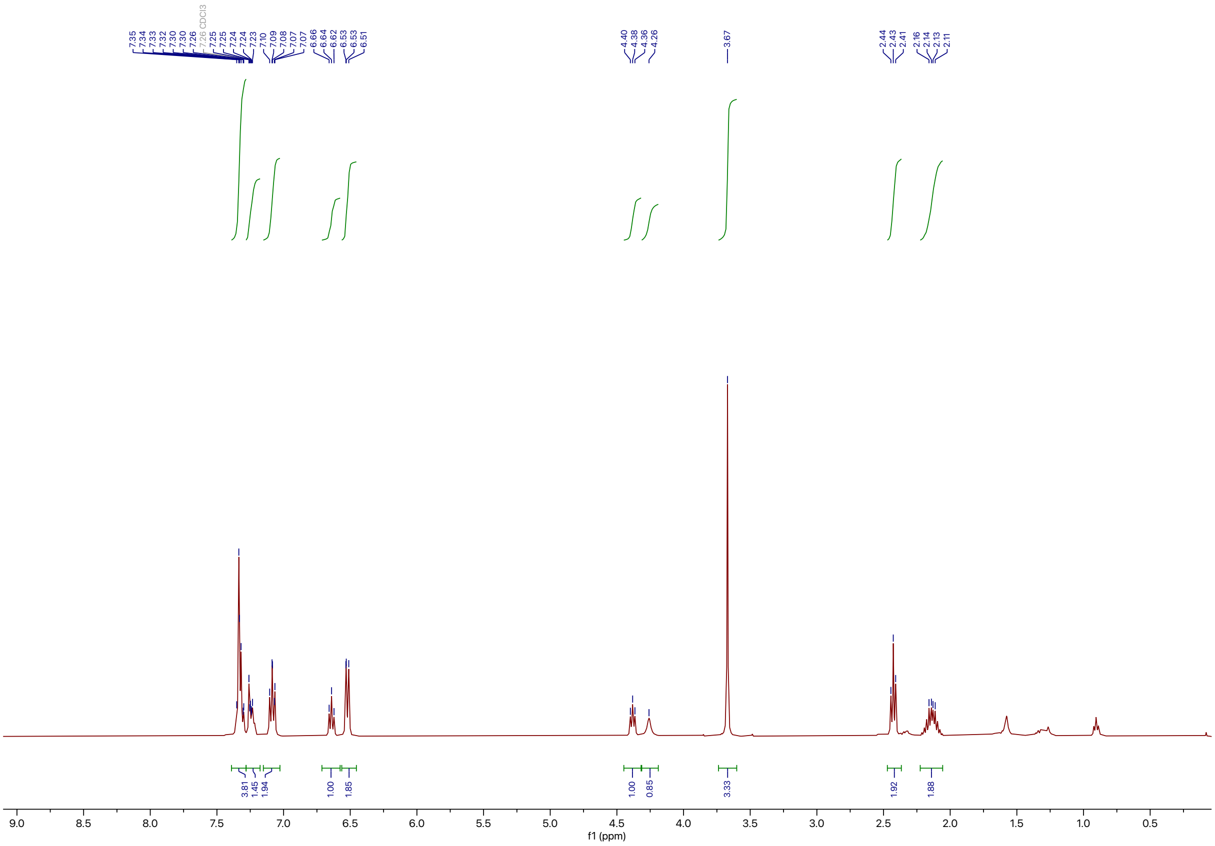

Figure S11. ^{1}H NMR of methyl 4-phenyl-4-(phenylamino)butanoate (400 MHz, $CDCl_3$, 25°C).

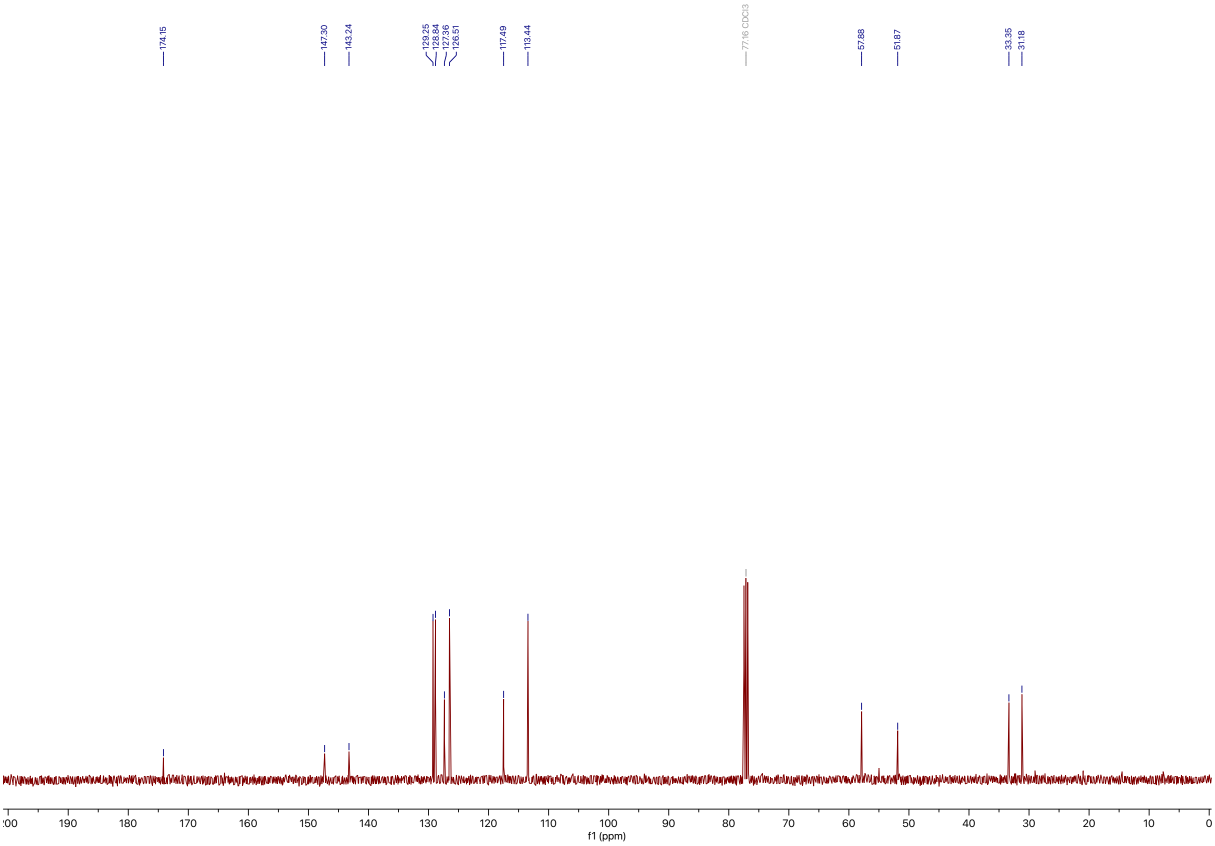

Figure S12. ^{13}C NMR of methyl 4-phenyl-4-(phenylamino)butanoate (101 MHz, $CDCl_3$, 25°C).

Kinetic curves of catalysis.

Following the procedures described above, we present here detailed kinetic curves that illustrate the progression of the reaction and the formation of the final product at various retention times. These curves provide a comprehensive visualization of the reaction dynamics, normalized using ^{1}H NMR yields to ensure accuracy and reproducibility. 1,3,5-trimethoxybenzene was employed as an internal standard to facilitate precise quantification, offering a reliable baseline for comparing the observed data across different experimental conditions.

* [2+2] intermolecular cycloaddition with complex [**2b**](PF_6) (0.5 mol%, 0.2 M in CH_2Cl_2).

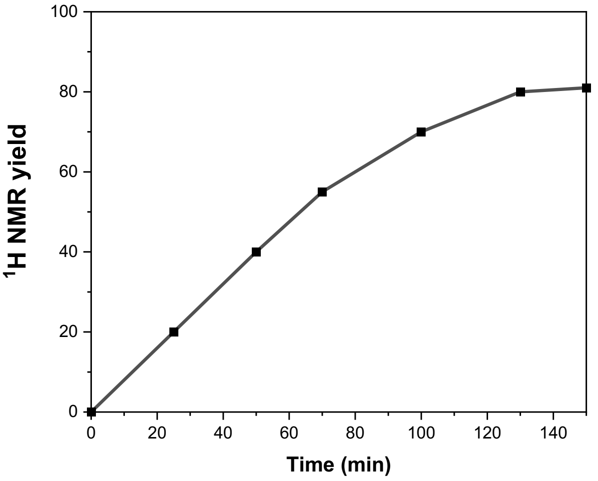

Figure S13. Trend-curves of formation of the desired product at different retention times.

* [2+2] intramolecular cycloaddition with complex [**2b**](PF_6) (0.5 mol%, 0.1 M in CH_3CN).

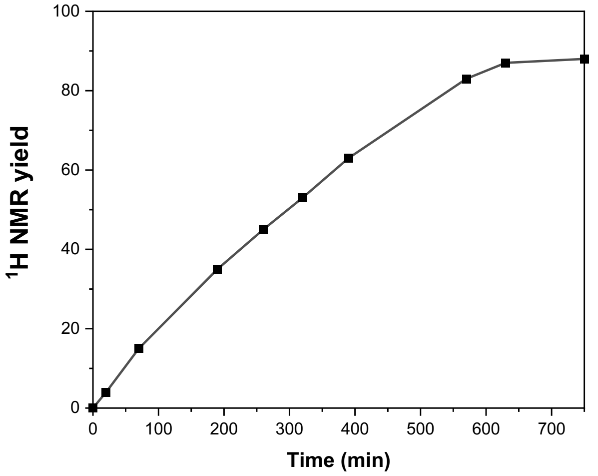

Figure S14. Trend-curves of formation of the desired product at different retention times.

VII) NMR spectra

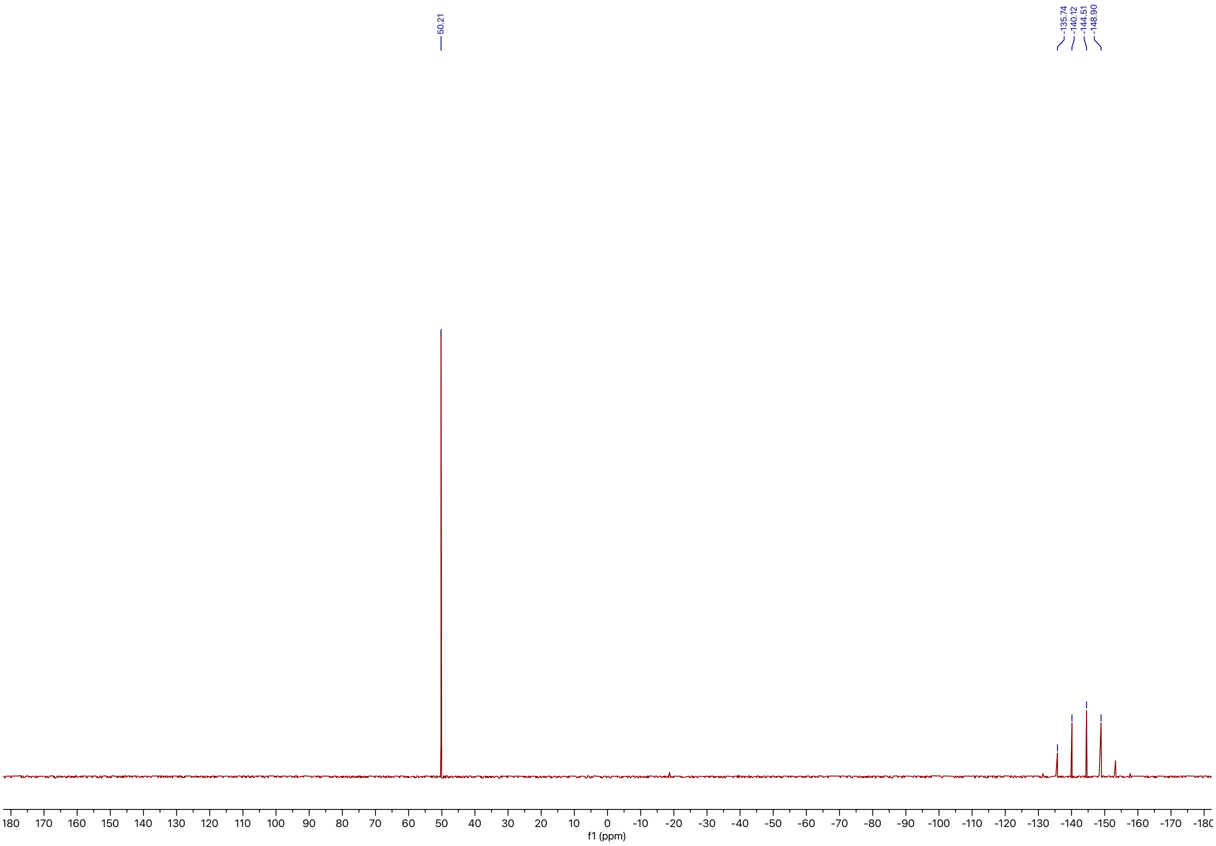

Figure S15. ^{31}P NMR of [**2a**](PF_6) (162 MHz, CD_2Cl_2, 25°C).

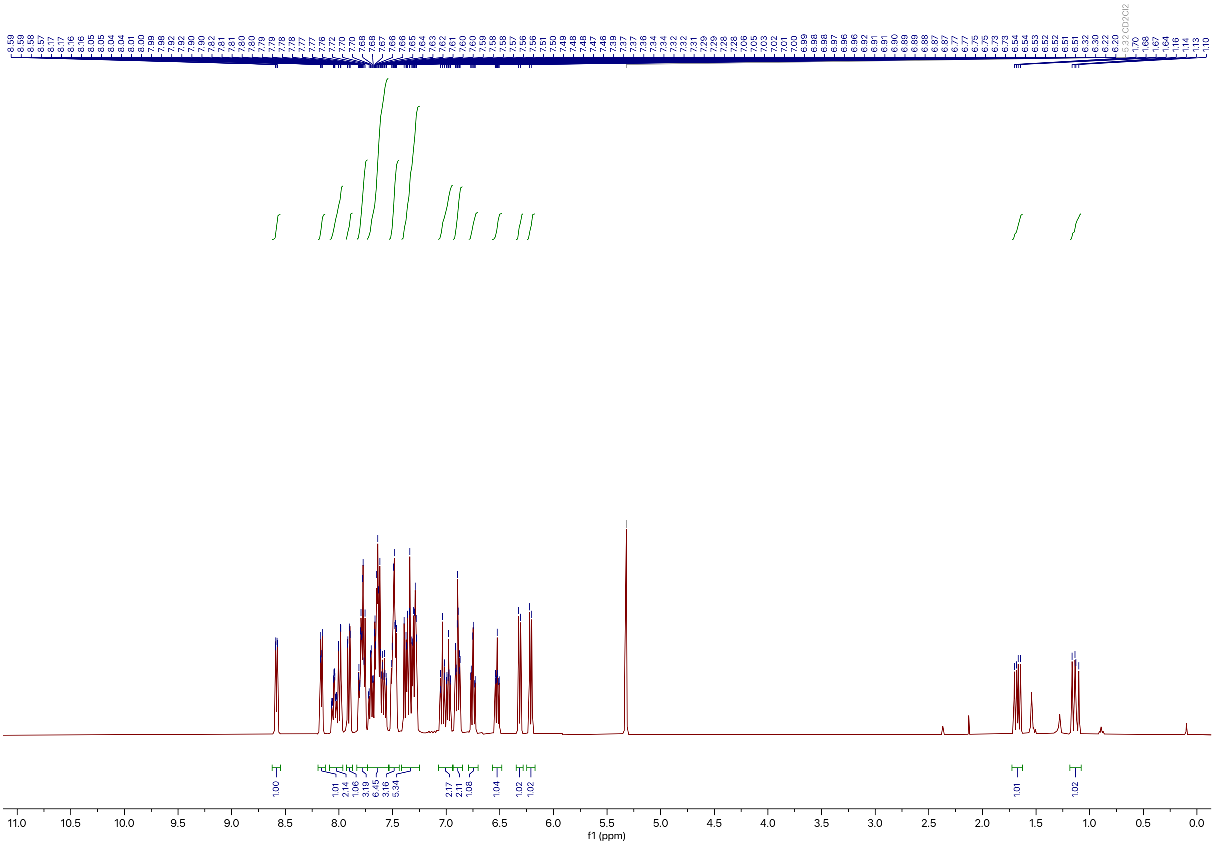

Figure S16. ^{1}H NMR of [**2a**](PF_6) (400 MHz, CD_2Cl_2, 25°C).

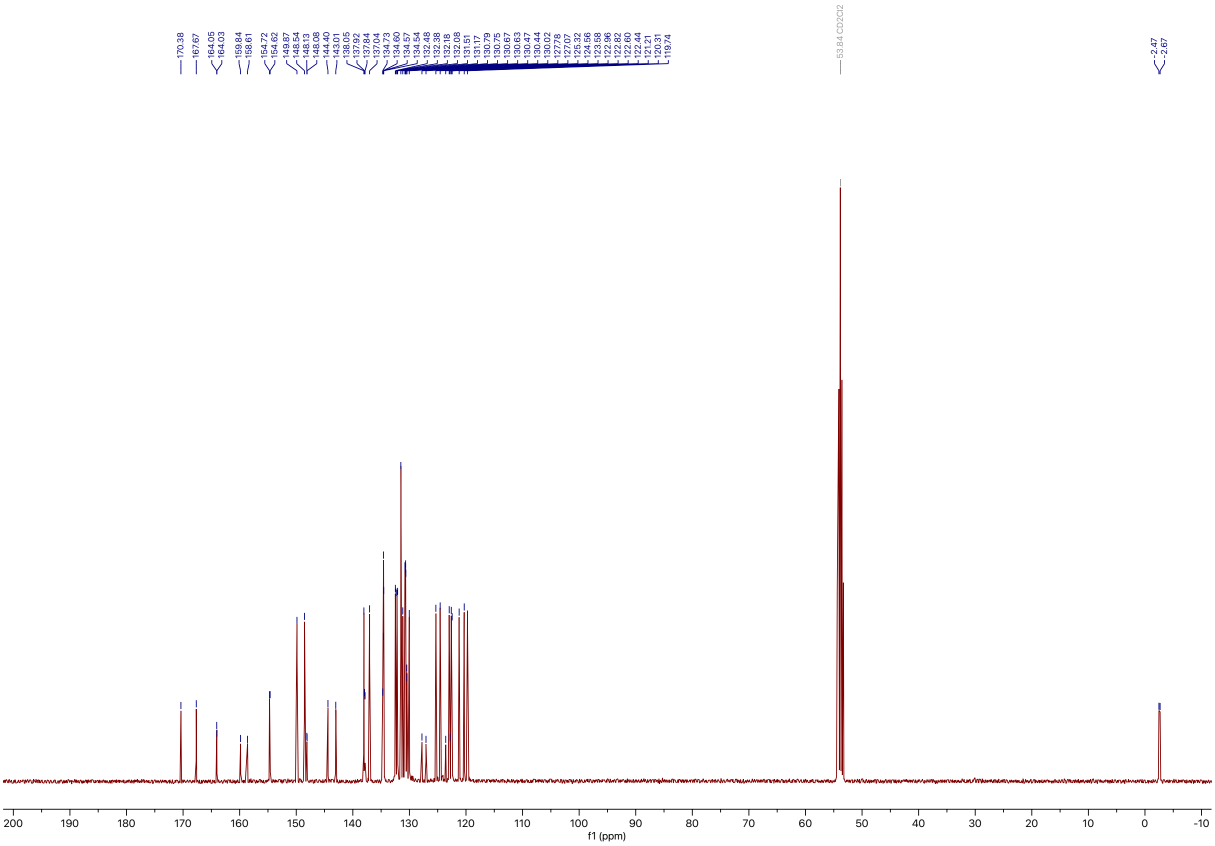

Figure S17. ^{13}C NMR of [**2a**](PF$_6$) (101 MHz, CD$_2$Cl$_2$, 25°C).

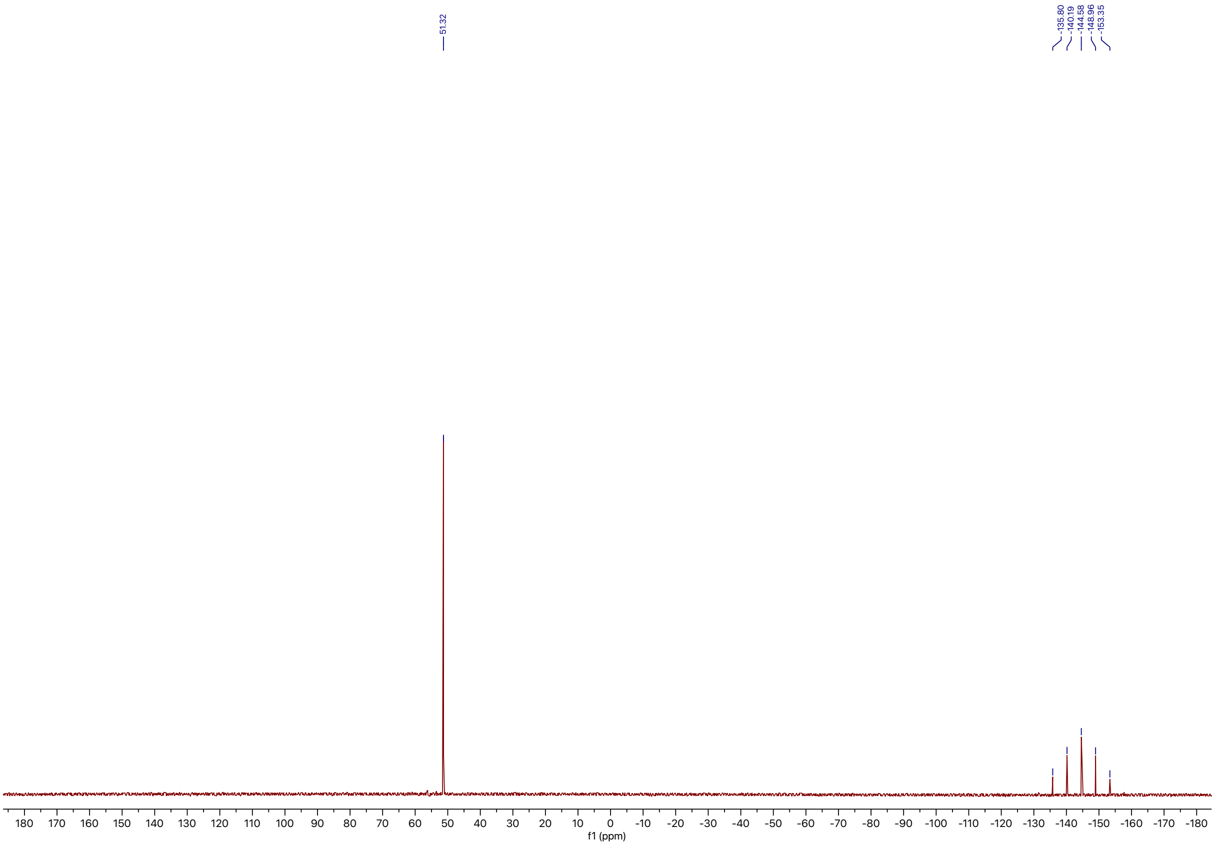

Figure S18. ^{31}P NMR of [**2b**](PF$_6$) (162 MHz, CD$_2$Cl$_2$, 25°C).

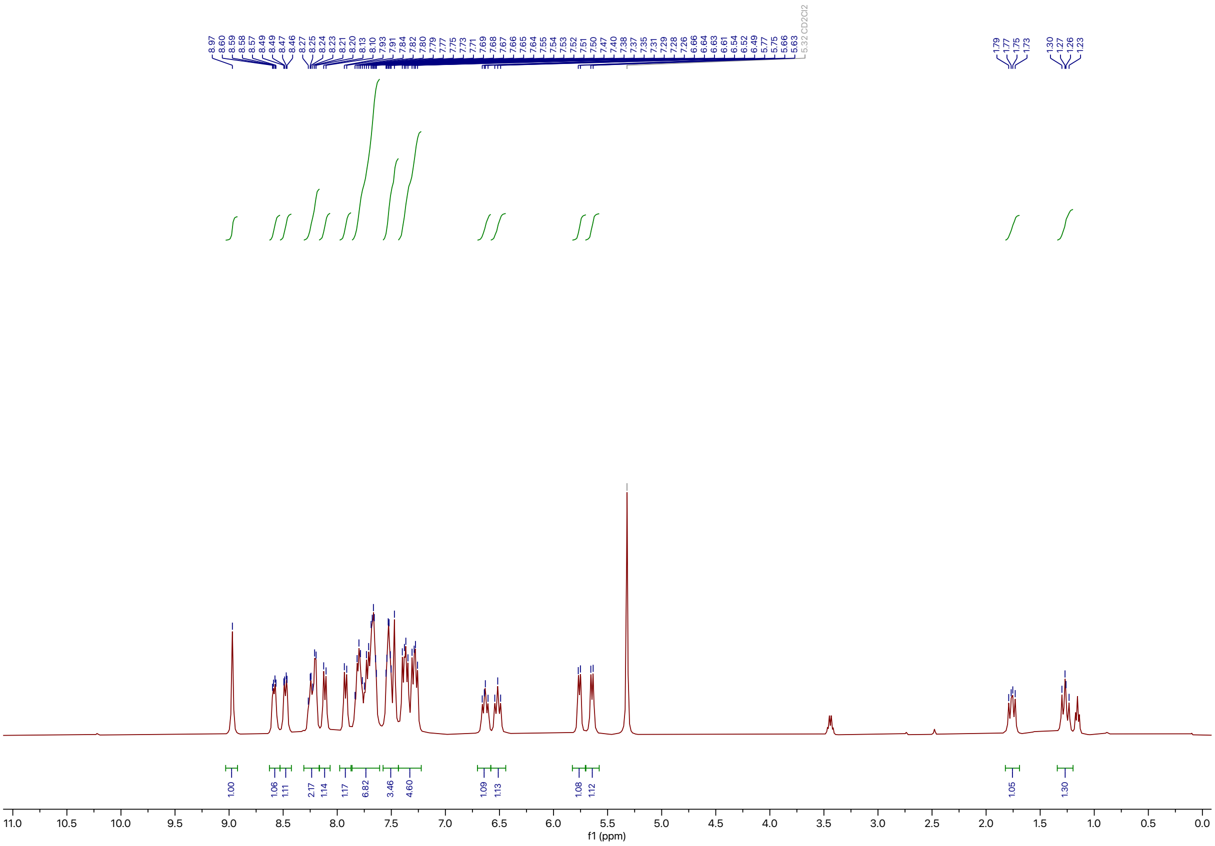

Figure S19. ^{1}H NMR of [**2b**](PF_6) (400 MHz, CD_2Cl_2, 25°C).

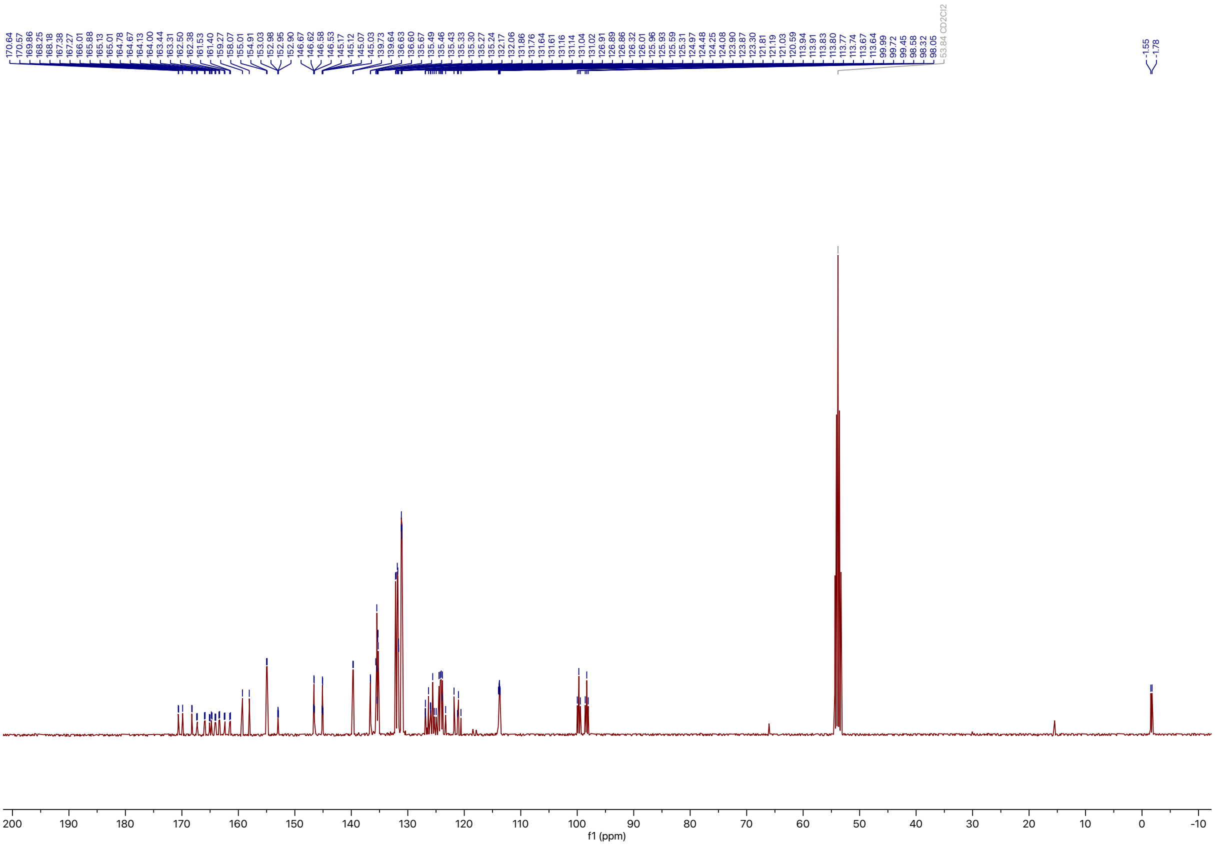

Figure S20. ^{13}C NMR of [**2b**](PF_6) (101 MHz, CD_2Cl_2, 25°C).

VIII) References

[1] M. Oderinde, *Org. Synth.*, 2017, **94**, 77−92.

[2] O. Fayafrou, E. Lognon, C. Duhayon, J.-B. Sortais, A. Monari, O. Baslé and Y. Canac, *Chem. Comm*. 2024, **60**, 13602−13605.

[3] G. M. Sheldrick, *Acta Cryst.*, 2015, **A71**, 3−8.

[4] P. W. Betteridge, J. R. Carruthers, R. I. Cooper, K. Prout and D. J. Watkin, *J. Appl. Cryst.*, 2003, **36**, 1487.

[5] G. M. Sheldrick, *Acta Cryst.*, 2008, **A64**, 112−122.

[6] Q. Lefebvre, R. Porta, A. Millet, J. Jia and M. Rueping, *Chem. Eur. J.*, 2020, **26**, 1363−1367.